J|A|C|S
ARTICLES
Published on Web 08/26/2005

Two States and Two More in the Mechanisms of Hydroxylation and Epoxidation by Cytochrome P450

Hajime Hirao,[†] Devesh Kumar,[†] Walter Thiel,[‡] and Sason Shaik*,[†]

Contribution from the Department of Organic Chemistry and the Lise Meitner-Minerva Center for Computational Quantum Chemistry, The Hebrew University of Jerusalem, 91904 Jerusalem, Israel, and The Max-Planck-Institut für Kohlenforschung, Kaiser-Wilhelm-Platz 1, D-45470 Mülheim an der Ruhr, Germany

Received June 11, 2005; E-mail: sason@yfaat.ch.huji.ac.il

Abstract: Past studies have shown that oxidation reactions by P450 Compound I (Cpd I) can be described by two competing quartet and doublet spin states, which possess three unpaired electrons, hence tri-radicals. One electron excitation from the δ orbital to σ^*_{xy} generates two states that possess five unpaired electrons, so-called penta-radicals, in sextet and quartet situations, and which were shown by theory to lie only ~12−14 kcal/mol higher in energy than the tri-radical ground states (ref 7). The present study focuses on the C−H hydroxylation and C═C epoxidation of propene by these penta-radical states. It is shown that the initial energy differences, between the penta-radical and tri-radical states, diminish along the reaction pathway, due to the favorable and cumulative exchange stabilization of the more open-shell species. Furthermore, theory suggests that hydrogen bonding to the thiolate ligand, and general polarity of the environment, reduce these gaps further, thereby making the penta-radical states accessible to ground-state reactivity. The interconversion between the tri-radical and penta-radical states along the reaction coordinate will depend on the dynamics of spin-flips and energy barriers between the sates. Especially interesting should be the region of the reaction intermediates; for both epoxidation and hydroxylation, this region is typified by a dense manifold of spin states and electromeric states (that differ by the oxidation state of iron), such that the total reactivity would be expected to reflect the interplay of these states, giving rise to multistate reactivity.

1. Introduction

Cytochromes P450 (P450s) constitute a family of ubiquitous metabolizing enzymes that catalyze oxygenation reactions of a variety of substrates, e.g., hydroxylation, epoxidation, hetero-atom oxidation, etc.[1] The richness of its reactivity and the many puzzles it generated[2] have made this enzyme a target for intense experimental and computational research. Theoretical studies revealed a two-state reactivity (TSR) in a variety of C−H hydroxylation and C═C epoxidation processes.[3−5] The origin of TSR was traced to the fact that the ground state of the active species, Compound I (Cpd I), has a virtually degenerate pair of so-called A_{2u} states, with quartet and doublet spins, shown as ^{2}**1** and ^{4}**1** in the orbital diagram in Scheme 1a. Little attention has been paid to the corresponding pair of sextet and quartet states, ^{6}**1′** and ^{4}**1′**, in Scheme 1b, which involve excitation of one electron from the low-lying δ orbital to the higher-lying σ^*_{xy} orbital. At first glance, this state seems to be too high to matter due to the large $\delta-\sigma^*_{xy}$ orbital energy gap, and as a result of this impression it has usually been neglected as an accessible state for reactivity studies.

The sextet state was mentioned briefly in the study by Yoshizawa et al. who performed DFT calculations for the hydroxylation reaction between Cpd I and ethane.[6] In this study, the sextet state was reported to lie higher in energy than the pair of doublet and quartet ground states of Cpd I by as much as 40.3 kcal/mol. Recently, Schöneboom et al.[7] reported B3LYP and QM(B3LYP)/MM calculations of Cpd I P450 and pointed

[†] The Hebrew University of Jerusalem.
[‡] The Max-Planck-Institut für Kohlenforschung.

(1) Ortiz de Montellano, P. R. Ed. *Cytochrome P450: Structure, Mechanisms and Biochemistry*, 3rd ed.; Plenum Press: New York, 2004.
(2) (a) Groves, J. T. Models and Mechanisms of Cytochrome P450 Action. In *Cytochrome P450: Structure, Mechanisms and Biochemistry*, 3rd ed.; Ortiz de Montellano, P. R., Ed.; Plenum Press: New York, 2004; Chapter 1. (b) Groves, J. T. *J. Chem. Educ.* **1985**, *62*, 928−931. (c) Sono, M.; Roach, M. P.; Coulter, E. D.; Dawson, J. H. *Chem. Rev.* **1996**, *96*, 2841−2888. (d) Newcomb, M.; Toy, P. H. *Acc. Chem. Res.* **2000**, *33*, 449−455. (e) Ortiz de Montellano, P. R.; de Voss, J. J. *Nat. Prod. Res.* **2002**, *19*, 471−493.
(3) (a) Shaik, S.; Cohen, S.; de Visser, S. P.; Sharma, P. K.; Kumar, D.; Kozuch, S.; Ogliaro, F.; Danovich, D. *Eur. J. Inorg. Chem.* **2004**, *35*, 207−226. (b) Shaik, S.; de Visser, S. P. Computational Approaches to Cytochrome P450 Actions. In *Cytochrome P450: Structure, Mechanisms and Biochemistry*, 3rd ed.; Ortiz de Montellano, P. R., Ed., Plenum Press: New York, 2004; Chapter 2, pp 45−86. (c) Meunier, B.; de Visser, S. P.; Shaik, S. *Chem. Rev.* **2004**, *104*, 3947−3980. (d) Shaik, S.; Kumar, D.; de Visser, S. P.; Altun, A.; Thiel, W. *Chem. Rev.* **2005**, *105*, 2279−2328.
(4) Shaik, S.; Filatov, M.; Schröder, D.; Schwarz, H. *Chem. Eur. J.* **1998**, *4*, 193−199.
(5) (a) Ogliaro, F.; Harris, N.; Cohen, S.; Filatov, M.; de Visser, S. P.; Shaik, S. *J. Am. Chem. Soc.* **2000**, *122*, 8977−8989. (b) de Visser, S. P.; Ogliaro, F.; Harris, N.; Shaik, S. *J. Am. Chem. Soc.* **2001**, *123*, 3037−3047. (c) de Visser, S. P.; Ogliaro, F.; Sharma, P. K.; Shaik, S. *J. Am. Chem. Soc.* **2002**, *124*, 11809−11826. (d) Ogliaro, F.; Cohen, S.; de Visser, S. P.; Shaik, S. *J. Am. Chem. Soc.* **2000**, *122*, 12892−12893. (e) Kumar, D.; de Visser, S. P.; Sharma, P. K.; Cohen, S.; *J. Am. Chem. Soc.* **2004**, *126*, 1907−1920. (f) Kamachi, T.; Yoshizawa, K. *J. Am. Chem. Soc.* **2003**, *125*, 4652−4661.
(6) Yoshizawa, K.; Shiota, Y.; Kagawa, Y. *Bull. Chem. Soc. Jpn.* **2000**, *73*, 2669−2673.
(7) Schöneboom, J. C.; Neese, F.; Thiel, W. *J. Am. Chem. Soc.* **2005**, 127, 5840−5853.

Scheme 1. Key Orbitals and Electronic Structures for the Ground States of Cpd I, ^{2,4}1 (in a), and the Two Excited States, ^{6,4}1′ (in b)

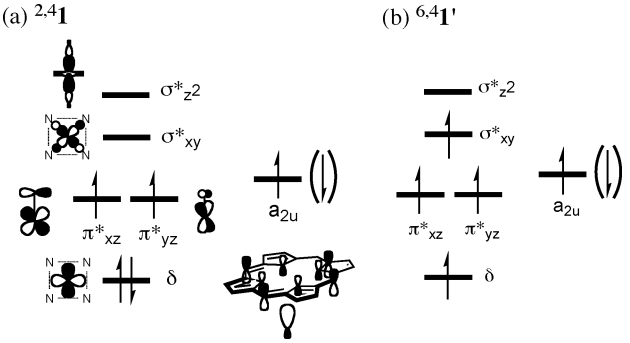

Scheme 2. Reaction Pathways and Labels of Critical Structures during Propene Epoxidation and Hydroxylation by the Low-lying States of Cpd I Shown in Scheme 1

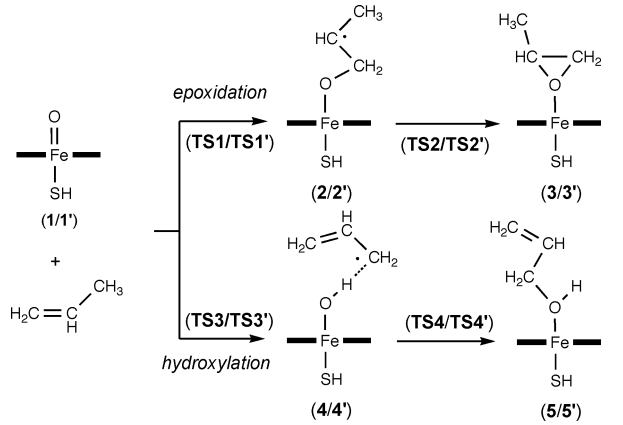

out that there exists a low-lying ^{6}**1′** state, which is just 14.8 kcal/mol higher than the ^{2,4}**1** ground states in the gas phase, and even lower, 12.0 kcal/mol, in the protein environment. Furthermore, the studies of analogous species by means of highly correlated ab initio methods[7] indicated that this energy gap of 12 kcal/mol might well be overestimated. Indeed, as suggested by Schöneboom et al.,[7] this result implies that the sextet state, ^{6}**1′**, and its antiferromagnetic ^{4}**1′** counterpart, could play a role, unconsidered before, in the multistate reactivity of Cpd I. This is precisely the subject of the present paper, which evaluates the importance of these higher-energy states, ^{6,4}**1′**, during C−H hydroxylation and C═C epoxidation of propene, as depicted in Scheme 2. As shall be demonstrated, the sextet state is low-lying throughout the reaction pathway, and may play a role in the reactivity of the enzyme. Analyses of these results will be provided in terms of the balance between orbital energies and the d−d exchange stabilization of high-spin situations.

2. Computational Details

By reference to Scheme 2, Cpd I was modeled as an iron−oxo porphine complex, and the proximal ligand was represented by SH^-. We report the energy profiles of epoxidation and hydroxylation for the ^{2,4}**1** and ^{6,4}**1′** states. The ground-state data for ^{2,4}**1** are mostly taken from an earlier study by one of us[5c] except that the energies are now also evaluated with a more extended basis set (see below).

We applied the same computational method as in our previous studies.[5a−d] All calculations were carried out with the unrestricted B3LYP method[8] using the Jaguar 4.2[9] and Gaussian 98[10] program packages. Since these two packages give essentially the same energetic values (differences up to ∼0.2 kcal/mol),[5c] we adopted the Jaguar energies and the Gaussian zero-point energies (ZPEs) throughout this paper. Geometry optimizations were performed with the LACVP basis set[11] on iron and the 6-31G basis set on the other atoms (B3LYP/LACVP(Fe), 6-31G(rest)), henceforth, B1. The B1 geometry optimization was followed by frequency calculations to characterize local minima and transition states (TS). Single-point calculations were subsequently performed with B2, the LACVP++**(Fe), 6-31++G**-(rest) basis set, which is a double-ζ basis set augmented with polarization and diffuse functions on all atoms. The effect of hydrogen bonding between the protein backbone and the thiolate ligand,[12] was mimicked in the same way as before [5c] by adding two ammonia molecules to the system at a fixed distance of $r_{S\cdots N} = 2.660$ Å. Bulk polarization effects were included, using the self-consistent reaction field (SCRF) model implemented in Jaguar 4.2, for a medium with a dielectric constant of $\epsilon = 5.7$ and a probe radius of 2.72 Å. Kinetic isotope effects (KIEs), during the hydroxylation process, were calculated as before,[5c] using the Eyring equation and the Wigner correction for tunneling. Orbitals were drawn by MOLEKEL 4.2.[13]

B3LYP is considered to overestimate the stability of high-spin states of iron complexes.[14] It was suggested that whenever this deficiency is apparent, it can be corrected by downsizing the effect of exchange stabilization due to inclusion of Hartree−Fock exchange.[14] A modification of B3LYP to B3LYP*, where the Hartree−Fock exchange was reduced by 5% (from 20% to 15%),[14] was demonstrated to lead to better agreement between theory and experiment of high-spin/low-spin energy gaps for hexacoordinate and sulfur-rich Fe(II) complexes, normally without deteriorating the results for other properties.[15] However, there are exceptions to the rule,[7,15−17] and in cases with high oxidation states, e.g., Fe(IV), B3LYP performs well,[16] while in other cases, analogous to Cpd I, this functional may even underestimate the stability of high-spin situations.[7] In view of this situation, we deemed it useful to test also the B3LYP* functional to assess the accuracy of B3LYP in the present context.

3. Results and Discussion

3.1. Cpd I. Figure 1 shows the key orbitals (Kohn−Sham orbitals, KSOs) for the sextet ^{6}**1′** state of Cpd I. Pairs of α and β KSOs of the same variety appear together and can be read as "one" orbital, which is doubly occupied in the case of a_{1u} and π_S, but only singly occupied otherwise. The unpaired electrons occupy the KSOs as depicted before in Scheme 1, namely, with single electron occupancy in a_{2u} and in four of the five d orbitals.

Figure 2 shows the lowest-lying states, their relative energies and key geometric parameters. With B3LYP, the states ^{6}**1′**/^{4}**1′**

(8) (a) Becke, A. D. *J. Chem. Phys.* **1992**, *96*, 2115−2160. (b) Becke, A. D. *J. Chem. Phys.* **1992**, *97*, 9173−9177. (c) Becke, A. D. *J. Chem. Phys.* **1993**, *98*, 5648−5652. (d) Lee, C.; Yang, W.; Parr, R. G. *Phys. Rev. B* **1988**, *37*, 785−789.
(9) *Jaguar 4.2*; Schrödinger, Inc.: Portland, OR, 2000.
(10) Frisch, M. J. et al. *Gaussian 98*; Gaussian, Inc.: Pittsburgh, PA, 1998
(11) (a) Hay, J. P.; Wadt, W. R. *J. Chem. Phys.* **1985**, *82*, 299−310. (b) Friesner, R. A.; Murphy, R. B.; Beachy, M. D.; Ringlanda, M. N.; Pollard, W. T.; Dunietz, B. D.; Cao, Y. *J. Phys. Chem. A* **1999**, *103*, 1913−1928.
(12) Poulos, T. L. *J. Biol. Inorg. Chem.* **1996**, *1*, 356−359.
(13) (a) Flükiger, P.; Lüthi, H. P.; Portmann, S.; Weber, J. *MOLEKEL 4.2*; Swiss Center for Scientific Computing: Manno, Switzerland, 2000−2002. (b) Portmann, S.; Lüthi, H. P. *CHIMIA* **2000**, *54*, 766−770.
(14) Reiher, M.; Salomon, O.; Hess, B. A. *Theor. Chem. Acc.* **2001**, *107*, 48−55.
(15) (a) Salomon, O.; Reiher, M.; Hess, B. A. *J. Chem. Phys.* **2002**, *117*, 4729−4737. (b) Harvey, J. N. *Struct. Bonding* **2004**, *112*, 151−183. (c) Smith, D. M.; Dupuis, M.; Straasma, T. P. *Mol. Phys.* **2005**, *103*, 273−278.
(16) (a) Ghosh, A.; Persson, B. J.; Taylor, P. R. *J. Biol. Inorg. Chem.* **2003**, *8*, 507−511. (b) Ghosh, A.; Taylor, P. R. *Curr. Opin. Chem. Biol.* **2003**, *7*, 113−124.
(17) (a) Schöneboom, J. C.; Thiel, W. *J. Phys. Chem. B* **2004**, *108*, 7468−7478. (b) Altun, A.; Thiel, W. *J. Phys. Chem. B* **2005**, *109*, 1268−1280. (c) Lin, H.; Schöneboom, J. C.; Cohen, S.; Shaik, S.; Thiel, W. *J. Phys. Chem. B* **2004**, *108*, 10083−10088.

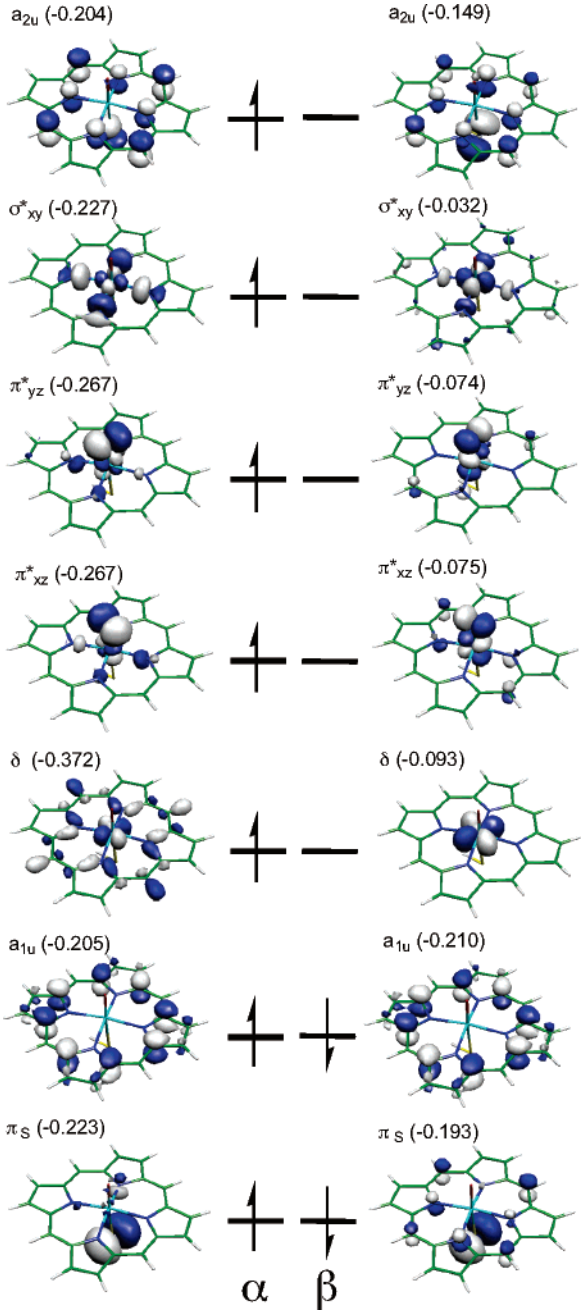

Figure 1. Key Kohn−Sham α and β orbitals for the ^{6}**1′** state. Energies are in units of hartree, but the vertical position of the orbital does not represent relative energies. Matching pairs of α and β orbitals are placed at the same height for simplicity.

lie 14.2/14.3 (B1) and 12.6/12.4 (B2) kcal/mol above the pair of ground states, ^{4,2}**1**, in good accord with the QM/MM calculations.[7] We use the slanted prime symbol in ^{6}**1′** and ^{4}**1′** to distinguish these states from the ground states, ^{2}**1** and ^{4}**1**; this symbol will characterize all the sextet and quartet state species nascent from ^{6}**1′** and ^{4}**1′**, respectively. Another sextet state, ^{6}**1**$_{z^2}$, in which the fifth electron occupies the $\sigma^*_{z^2}$ orbital was found to lie above ^{6}**1′** by about 18 kcal/mol with B1, because in Cpd I, $\sigma^*_{z^2}$ is higher in energy than σ^*_{xy} due to the short Fe−O bond. This is in contrast to the situation of the product complexes, where the Fe−O distance is much longer, and accordingly, $\sigma^*_{z^2}$ descends lower in energy than σ^*_{xy}.[5c] As such, we will focus, hereafter, on the sextet state that involves σ^*_{xy} occupancy.

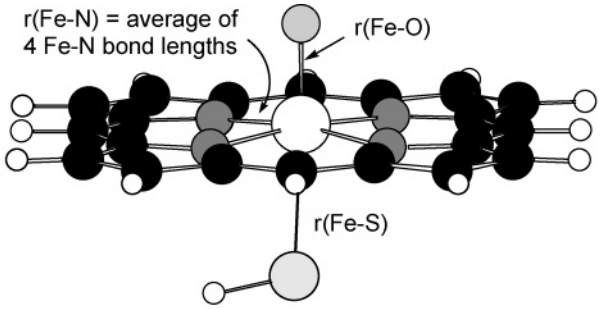

state	singly occupied orbitals	E_{rel} B1 (B2//B1) B3LYP	E_{rel} B1 B3LYP*// B3LYP	r(Fe-O)	r(Fe-S)	r(Fe-N)
^{2}**1**	$\pi^*\pi^*a_{2u}$	0.1 (-0.1)	-0.1	1.648	2.604	2.017
^{4}**1**	$\pi^*\pi^*a_{2u}$	0.0 (0.0)	0.0	1.651	2.586	2.017
^{4}**1'**	$\delta\pi^*\pi^*\sigma^*_{xy}a_{2u}$	14.2 (12.4)	16.7	1.659	2.644	2.081
^{6}**1'**	$\delta\pi^*\pi^*\sigma^*_{xy}a_{2u}$	14.3 (12.6)	16.5	1.654	2.570	2.080
^{6}**1**$_{z^2}$	$\delta\pi^*\pi^*\sigma^*_{z^2}a_{2u}$	32.2 (34.8)	35.0	1.785	3.037	2.035

Figure 2. Relative energies (E_{rel}, in kcal/mol) and key bond lengths (in Å) of the states of Cpd I. The relative energies are shown for B3LYP and B3LYP*//B3LYP.

Table 1. B3LYP/B1 (out of parentheses) and B3LYP/B2//B1 (in parentheses) Values of Group Spin Densities of Cpd I in Various States

	Fe	O	Por	SH
^{2}**1**	1.17 (1.17)	0.93 (0.91)	−0.49 (−0.47)	−0.60 (−0.61)
^{4}**1**	1.04 (1.06)	0.98 (0.96)	0.43 (0.42)	0.55 (0.56)
^{4}**1′**	3.21 (3.23)	0.66 (0.65)	−0.35 (−0.33)	−0.52 (−0.55)
^{6}**1′**	3.03 (3.06)	0.70 (0.68)	0.85 (0.83)	0.43 (0.43)

According to B3LYP*, the states ^{6}**1′**/^{4}**1′** lie 16.5/16.7 kcal/mol above the ground state; these gaps are larger than those from B3LYP by 2−2.5 kcal/mol. Thus, as expected, reducing the contribution of the Hartree−Fock exchange indeed destabilizes the high-spin situations. However, high-level ab initio results[7] tend to give even smaller gaps than B3LYP in related model compounds, and one may thus doubt whether B3LYP* is indeed most suitable for our purposes (further discussion see below).

Table 1 collects the group spin densities in the ground states, ^{2,4}**1** and the two excited states, ^{6}**1′** and ^{4}**1′**; both B1 and B2 data are presented for each entry. According to Scheme 1b and Figure 1, the ^{6}**1′** and ^{4}**1′** states of Cpd I possess four unpaired electrons in d orbitals and one on the porphyrin center. Since the π^*-type d orbitals are delocalized onto the oxo ligand, and the σ^*_{xy}-type d orbital is delocalized toward the nitrogen atoms of the porphyrin, the computed spin densities on iron are smaller than 4 (ca. 3.0−3.2) while those on the FeO moiety are closer to 4 (ca. 3.7−3.9). In the ground states ^{2,4}**1,** the spin density on Fe is close to unity, for the same reason (orbital delocalization), but the FeO moiety carries spin density of 2.0, as expected from the occupancy of the d orbitals in Scheme 1a. The spin densities on the porphyrin and thiolate ligands in the ^{6}**1′** and ^{4}**1′** states have contributions from the singly occupied a_{2u} and σ^*_{xy} orbitals whose sum can exceed 1 as in ^{6}**1′** (1.28). By contrast, in the ground states, ^{2,4}**1**, the combined spin density on porphyrin and thiolate comes from a_{2u} and is close to unity (+1 or −1). Thus, the ground states ^{2,4}**1** are *tri-radicaloids* (with three unpaired

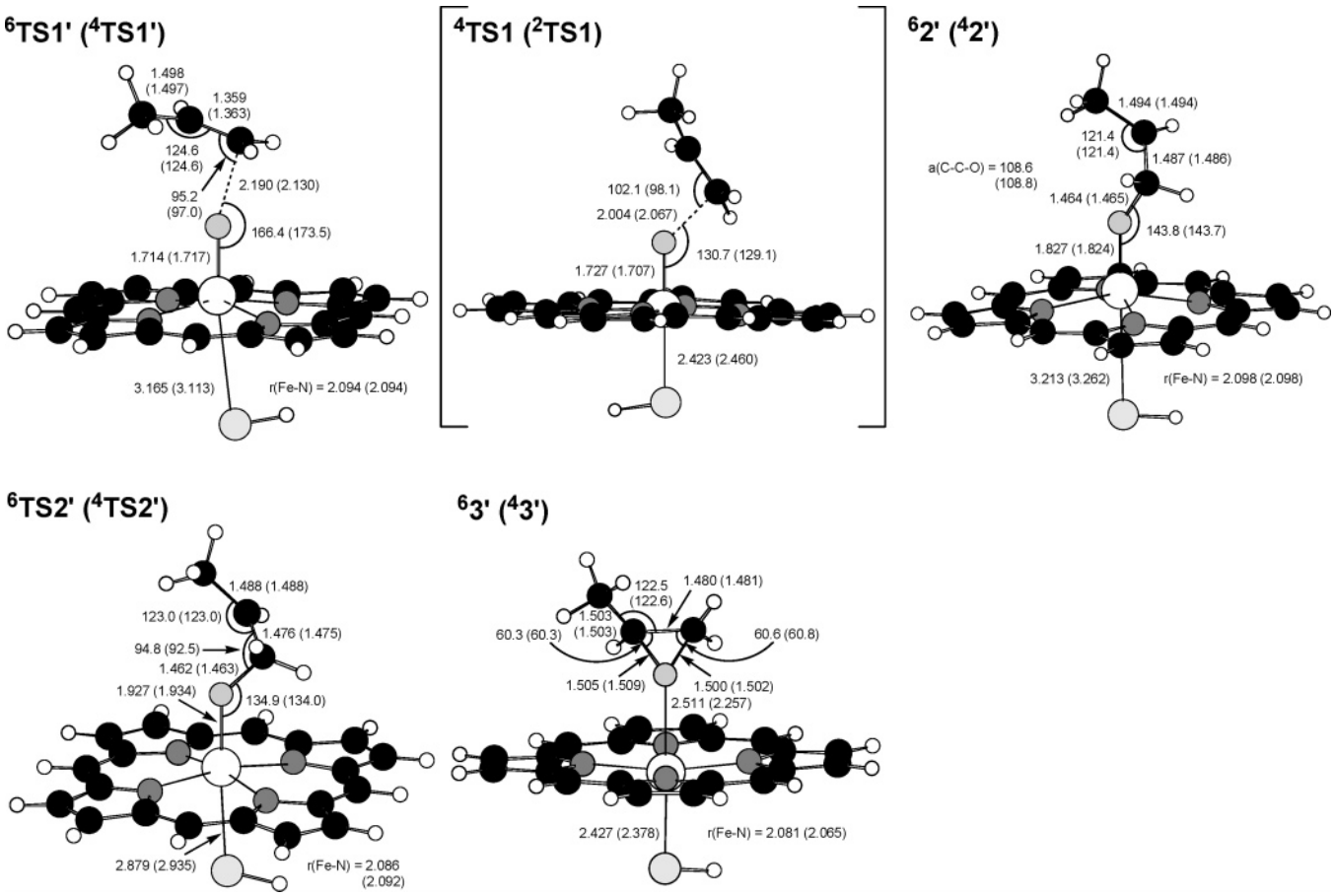

Figure 3. B3LYP/B1 optimized structures of critical species along the epoxidation pathways of the penta-radicaloid states. In square brackets are the ^{2,4}**TS1** species produced in the respective pathways of the tri-radicaloid states (ref 5c). All labels follow Scheme 2. Bond lengths are in Å and bond angles in degrees.

electrons), and the excited states ^{6,4}**1′** are *penta-radicaloids* (with five unpaired electrons).

3.2. Structure and Energy during C═C Epoxidation and C−H Hydroxylation of Propene. The structures of the transition states, intermediates, and product complexes along the oxidation pathways promoted by the penta-radicaloid states are shown in Figures 3 and 4. The bond activation transition states, ^{6}**TS1′** and ^{4}**TS1′** (Figure 3) and ^{6}**TS3′** and ^{4}**TS3′** (Figure 4), assume upright conformations with FeOC and FeOH angles of 170° or so, larger than in the sulfoxidation process described recently.[18] The corresponding structures, nascent from the ground-state reactions (of the tri-radicaloids, ^{4,2}**1**), are shown in the square brackets in Figures 3 and 4, and it is obvious that they all possess much smaller FeOC and FeOH angles compared to the structures in the excited states.

The corresponding gas-phase energy profiles for the two processes are depicted in Figure 5 at the B3LYP and B3LYP* levels. It is seen that profiles of the penta-radicaloid states nascent from ^{6,4}**1′** lie higher than the profiles of the ground states nascent from ^{2,4}**1**, at both levels. However, with B3LYP the sextet surface approaches the ground states and may thus become relevant for the reactivity. By contrast, with B3LYP* the profiles of the penta-radicaloid states are sufficiently higher than those of the tri-radicaloid states, to suggest that the former states should not be important in the reactivity.

Are the penta-radicaloid states relevant? As we noted above for the states of Cpd I, the modified B3LYP* functional seems to exaggerate the destabilization of the penta-radicaloid relative to that of the tri-radicaloid states. This tendency becomes more apparent for the product ferric alcohol complexes. Here energy differences between the low-spin ground state and the high-spin sextet state are 7.7 kcal/mol with B3LYP and 11.5 kcal/mol with B3LYP*. Experimental data on P450 reactions indicate that in the cases of the ferric alcohol complex, during camphor hydroxylation,[19] the ferric aqua resting state,[20,21] and in the pentaccordinate ferric complex of the enzyme,[20,22] there is spin equilibrium between the doublet and sextet states. Spin equilibrium requires energy differences of at most 2 kcal/mol. B3LYP and QM(B3LYP)/MM calculations of all these complexes[3d,17] predict correctly the ground state (e.g., doublet states in the ferric aqua and ferric alcohol complexes, and a sextet state in the case of the pentacoordinate ferric complex) and yield

(18) Kumar, D.; de Visser, S. P.; Sharma, P. K.; Hirao, H.; Shaik, S. *Biochemistry* **2005**, *44*, 8148−8158.

(19) (a) Lipscomb, J. D. *Biochemistry* **1980**, *19*, 3590−3599. (b) Davydov, R.; Makris, T. M.; Kofman, V.; Werst, D. E.; Sligar, S. G.; Hoffman, B. M. *J. Am. Chem. Soc.* **2001**, *123*, 1403−1405.

(20) (a) Tsai, R.; Yu, C. A.; Gunsalus, I. C.; Peisach, J.; Blumberg, W.; Orme-Johnson, W. H.; Beinert, H. *Proc. Natl. Acad. Sci. U.S.A.* **1970**, *66*, 1157−1163. (b) Sharrock, M.; Debrunner, P. G.; Schulz, C.; Lipscomb, J. D.; Marshall, V.; Gunsalus, I. C. *Biochim. Biophys. Acta* **1976**, *420*, 8−26. (c) Sligar, S. G. *Biochemistry* **1976**, *15*, 5399−5406. (d) Denisov, I. G.; Makris, T. M.; Sligar, S. G.; Schlichting, I. *Chem. Rev.* **2005**, *105*, 2253−2277.

(21) A synthetic ferric aqua complex with a thiophenoxide axial ligand has, in fact, a sextet ground state. See, Aissaoui, H.; Bachmann, R.; Schweiger, A.; Woggon, W.-D. *Angew. Chem., Int. Ed.* **1998**, *37*, 2998−3002.

(22) Auclair, K.; Moënne-Loccoz, P.; Ortiz de Montellano, P. R. *J. Am. Chem. Soc.* **2001**, *123*, 4877−4885.

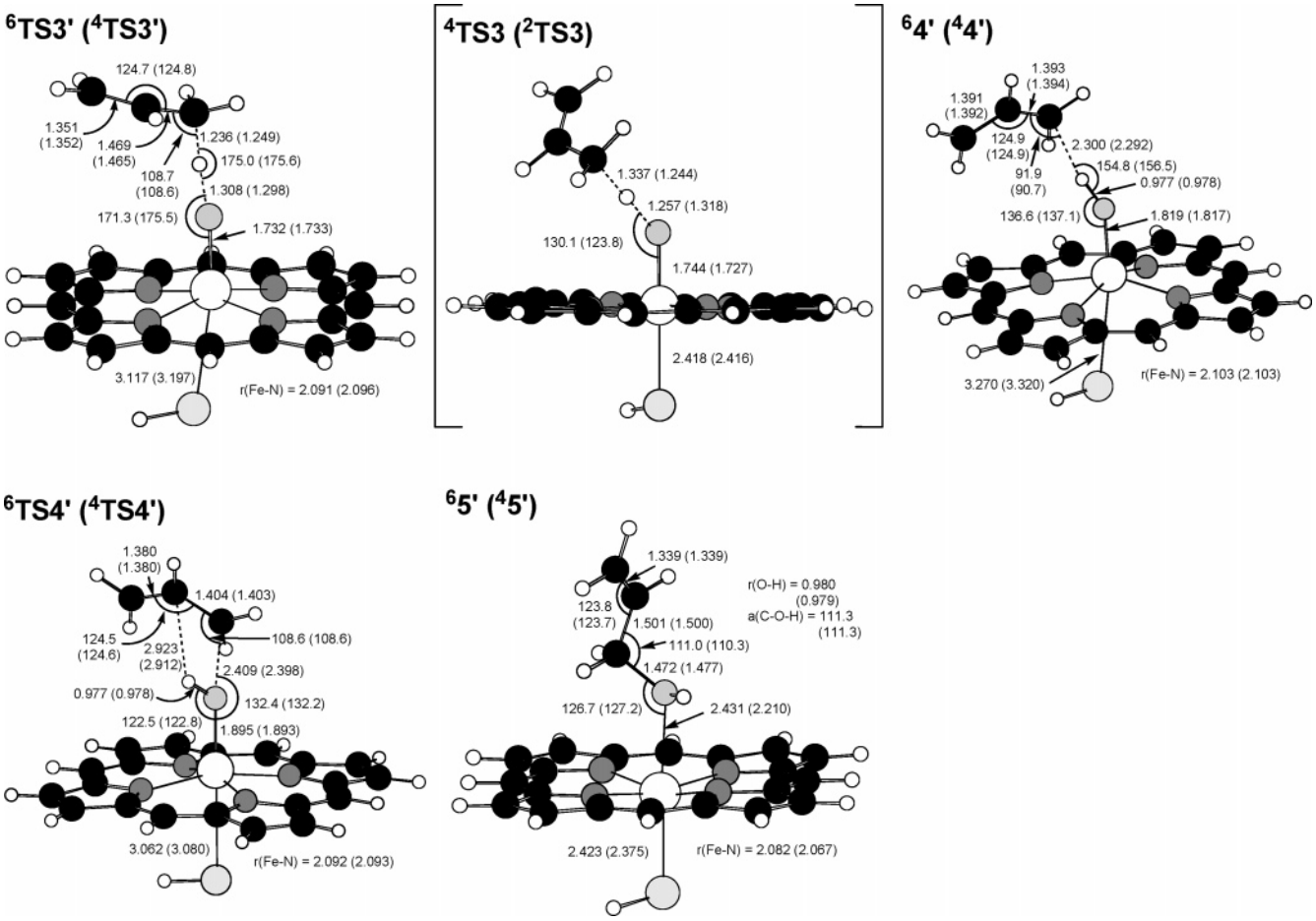

Figure 4. B3LYP/B1 optimized structures of critical species along the hydroxylation pathways of the penta-radicaloid states. In square brackets are the ^{2,4}**TS3** species produced in the respective pathways of the tri-radicaloid states (ref 5c). All labels follow Scheme 2. Bond lengths are in Å and bond angles in degrees.

small energy differences between the sextet and doublet spin states, but even these small differences are larger than the 2 kcal/mol limit. Thus, for example, for the ferric aqua complex, which has a doublet ground state and a higher-lying sextet state, the B3LYP calculated gap is 2.5−4.0 kcal/mol in the gas phase with basis sets larger than B1.[17a] Indeed, for the resting state, our calculations (see Supporting Information) show that with B2, the doublet−sextet gap is 5.2/9.1 kcal/mol with B3LYP/B3LYP* and becomes 1.0/5.4 kcal/mol when hydrogen bonding to thiolate and medium polarity are added. Still, the B3LYP* datum is too large to qualify for the experimental situation, whereas the B3LYP datum is in good agreement with experiment. The same applies to the ferric alcohol complexes of propene hydroxylation; here too, the B3LYP* energy difference is significantly larger than would be expected from experimental data on the hydroxy camphor complex. Thus, it appears that the B3LYP* functional is less suitable than B3LYP for the problem investigated here. We recall that the calibration of the Hartree−Fock exchange was done for ferrous, Fe(II), complexes,[14] whereas the correction of the exchange term may well be system dependent rather than an all-purpose correction.[15b] Another concern with the B3LYP* correction is that it is calibrated against experimental data and hence includes the effect of solvents on the low-spin/high-spin energy gap. As shown previously,[17b] the polarity of the protein pocket lowers considerably the energies of the high- and intermediate-spin states of ferric and ferrous complexes compared with the corresponding low-spin states. As such, gas-phase B3LYP* correction would tend to exaggerate the destabilization of the high-spin states relative to that of the low-spin states for such complexes as in our study. In accord with this assessment, the following discussions will rely on the B3LYP data.

Figure 6 shows the B3LYP/B2//B1 results without and with ZPE correction of the energies. It is seen that already in the gas phase, the energy difference between the species nascent from the penta- and tri-radicaloid states shrinks from 12 kcal/mol at the reactant state, to 5−6 kcal/mol at the bond activation transition states, and the intermediates, and to still smaller values (for sextet) at the product stage. ZPE correction further reduces these energy differences.

Adding two NH- - -S hydrogen bonds to the thiolate ligand, as in Figure 7, stabilizes, as noted before,[5c] the low-spin doublet TS species compared with the respective ferromagnetic quartet-state species (e.g., ^{2}**TS1** vs ^{4}**TS1**). However, the hydrogen bonds to the thiolate further reduce the energy differences between the four species, albeit not uniformly. Now, the intermediate complexes, **2** and **2′**, during epoxidation are all jammed within 2 kcal/mol, and the intermediates, **3** and **3′**, during hydroxylation maintain a gap of 5 kcal/mol.

Figure 8 shows the effect of including electronic polarization through a medium effect, using a dielectric constant, ϵ, of 5.7. It is seen that now the sextet ^{6}**TS1′** species, in C=C epoxidation, comes close to the low-spin doublet species and is now the second lowest **TS1** species. The hydroxylation

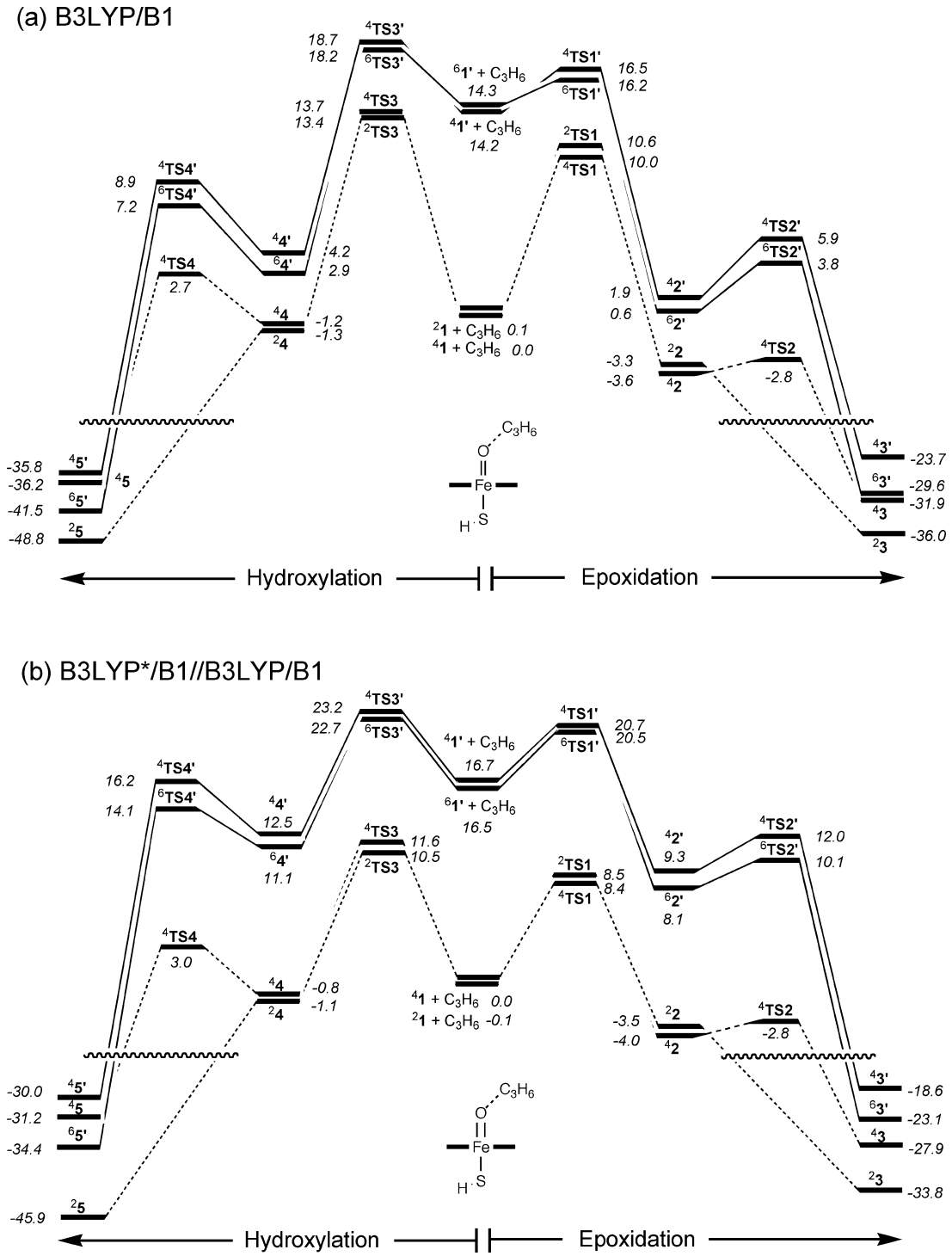

Figure 5. Energy profiles for epoxidation and hydroxylation of propene by the tri- and penta-radicaloid states of Cpd I. (a) B3LYP/B1 profiles. (b) B3LYP*/B1//B3LYP/B1 profiles.

process still prefers the low-spin path,[2] but the energy difference between the sextet ^{6}**TS3′** species and ^{4}**TS3** decreases to less than 1 kcal/mol (with ZPE). The most pronounced effect occurs at the stage of the intermediates. During epoxidation, the lowest-energy state is ^{6}**2′**, and the other states are distributed within 1−3 kcal/mol. Similarly, during hydroxylation, the ^{6}**4′** and ^{4}**4′** intermediates are very close or even lower (with ZPE) than the ones generated from the ground-state surfaces. A similar dense manifold is obtained for the product complexes. Clearly, based on the B3LYP results, the high-spin states nascent from **1′** should play a role in the reactivity of Cpd I species.

3.3. Spin Density Distribution along the Reaction Pathways. Following the Mulliken spin density along the reaction path provides some insight on the changes in the electronic structure. Tables 2 and 3 summarize the group spin densities for the critical structures of the two mechanisms; the spin densities of Cpd I are collected in Table 1.

As the reactions proceed, spin density gradually accumulates on the propene moiety, approaching 1 in the intermediate state.

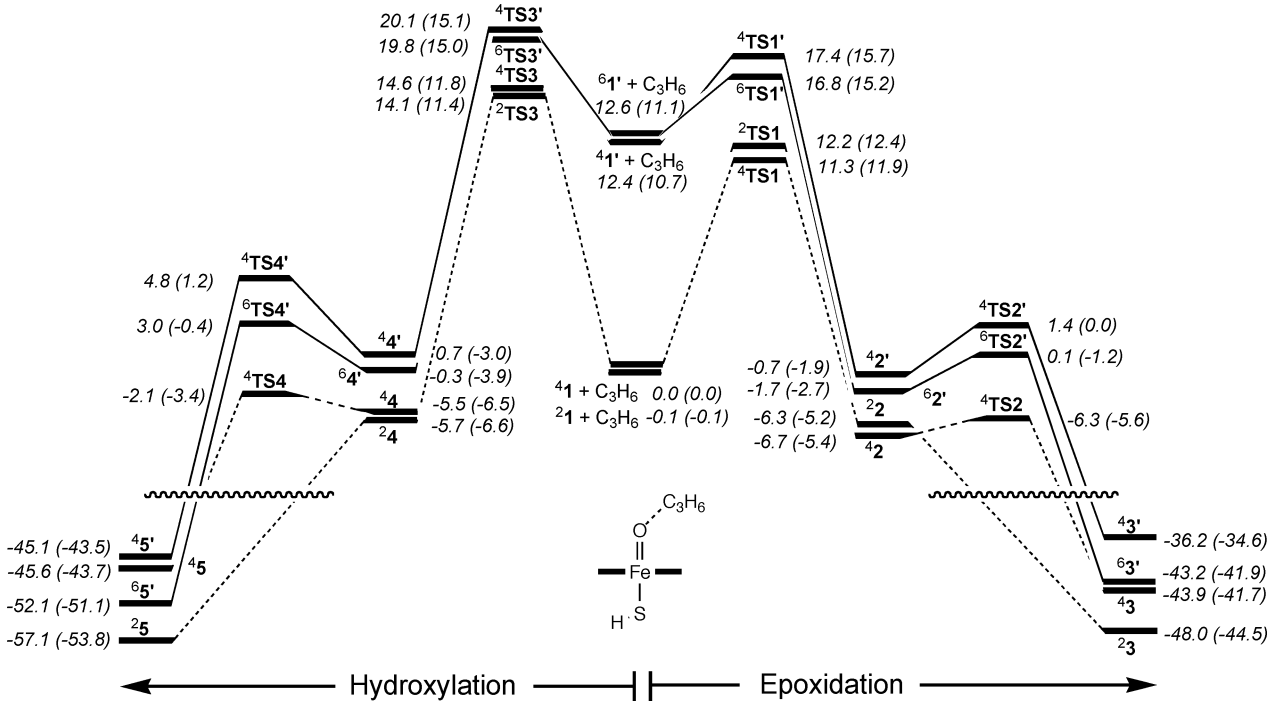

Figure 6. B3LYP/B2//B1 energy (kcal/mol) profiles along the epoxidation and hydroxylation. The structures for the reactions of ^{4}**1** and ^{2}**1** were taken from ref 5c. The values out of parentheses are energy values, while in parentheses the values include ZPE correction (taken from the B1 calculations). All labels follow Scheme 2.

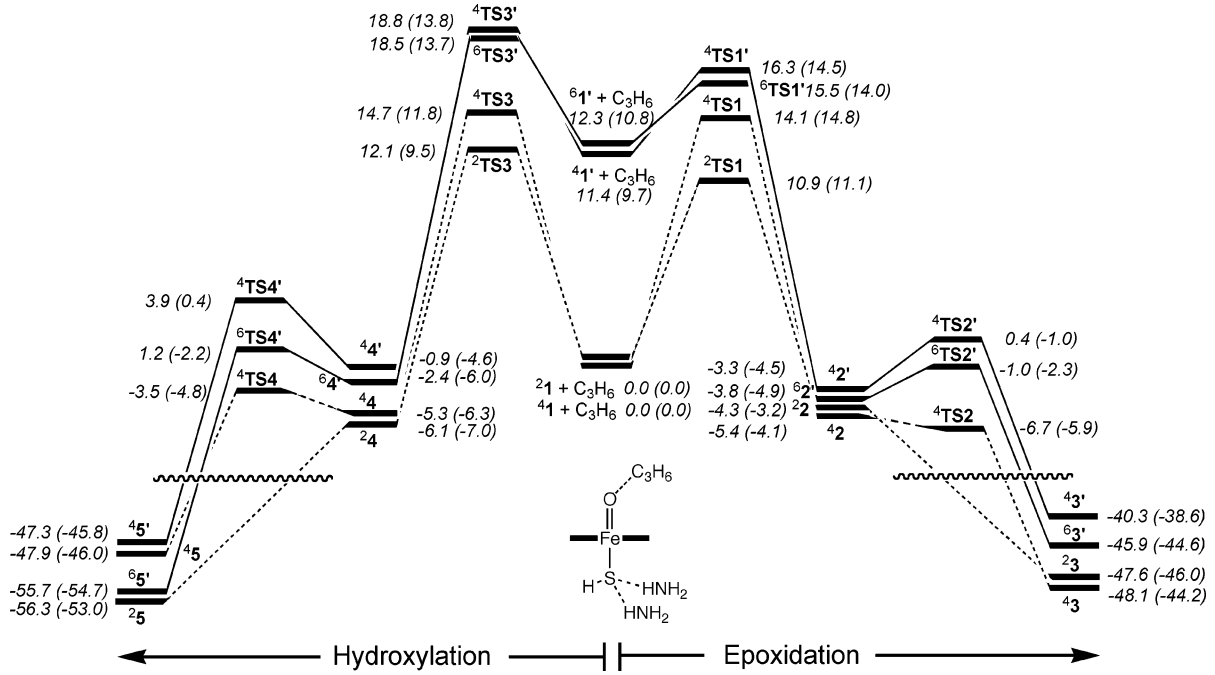

Figure 7. B3LYP/B2//B1 energy (kcal/mol) profiles along the epoxidation and hydroxylation pathways of the penta-radicaloid species using 2 NH- - -S to the thiolate ligand. The values out of parentheses are energy values, while in parentheses the values include ZPE correction taken from the bare species in Figure 6. All labels follow Scheme 2.

For the intermediates that are nascent from the penta-radicaloid states, the propene spin density is always negative, reaching −1. By contrast, in the tri-radicaloid states, the low-spin doublet has negative spin density on propene while in the quartet state the spin density is positive. Past the intermediates, the spin density on propene starts to decrease in the rebound processes, reaching zero in the product complexes.

3.4. Kinetic Isotope Effects (KIEs) for the Hydroxylation Pathways. Since the hydrogen abstraction transition states of the penta-radicaloid species, ^{4,6}**TS3′**, and the tri-radicaloid species, ^{2,4}**TS3**, are substantially different (see Figure 4), we calculated the KIEs for the corresponding processes when an allylic C−H bond is replaced by a C−D bond. The semi-classical Eyring/Wigner-corrected values are 5.6/7.1 for ^{2}**TS3** and 6.6/9.7 for ^{4}**TS3** in the tri-radicaloid case, but 5.6/7.1 for ^{4}**TS3′** and 5.3/6.5 for ^{6}**TS3′** in the penta-radicaloid case. These KIE trends reflect the position of the respective transition-state structures along the hydrogen transfer coordinate[5e]

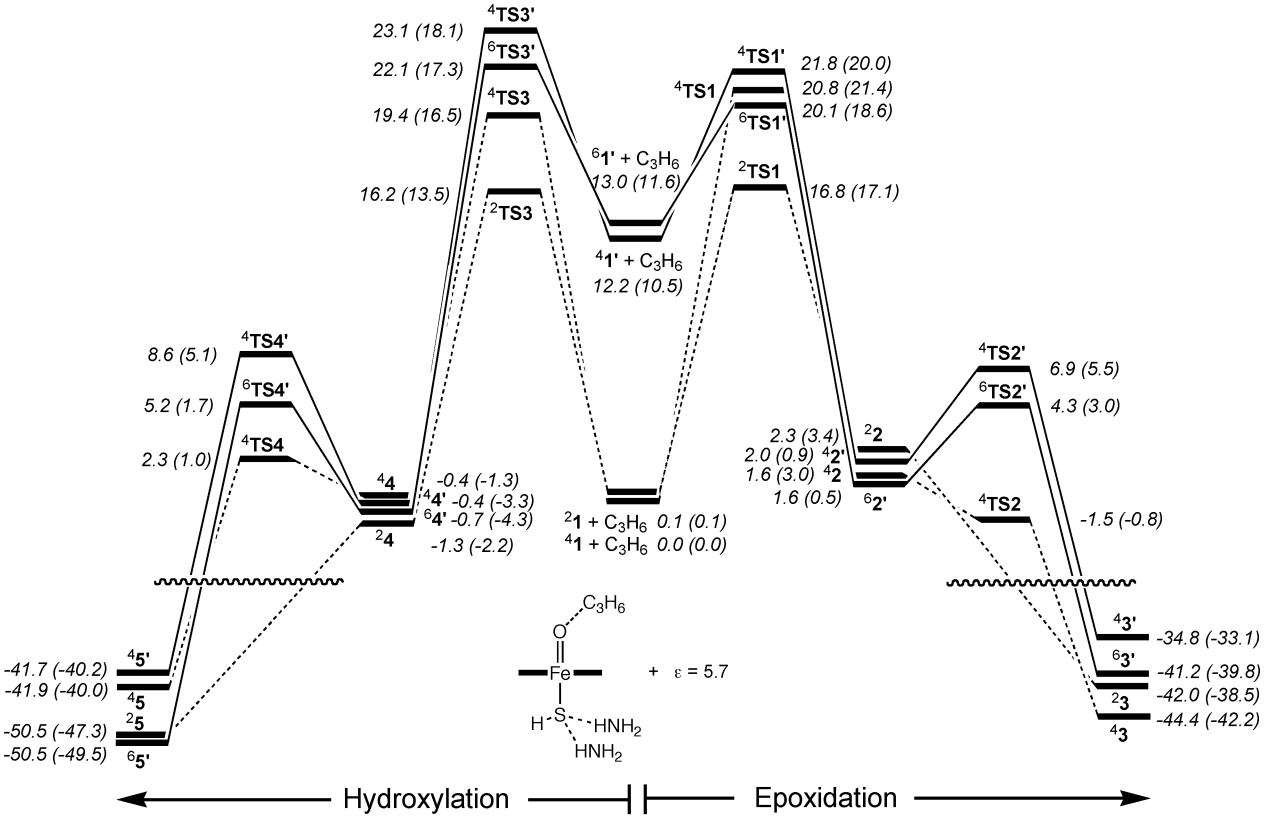

Figure 8. B3LYP/B2//B1 energy (kcal/mol) profiles along the epoxidation and hydroxylation pathways of the penta-radicaloid species, taking into account the effects of NH- - -S hydrogen bonds and polarization effect by a medium with a dielectric constant, $\epsilon = 5.7$. The values out of parentheses are energy values, while in parentheses the values include ZPE correction taken from the bare species in Figure 6. All labels follow Scheme 2.

Table 2. Group Spin Densities during Epoxidation at the B3LYP/B1 and B3LYP/B2//B1 (in Parentheses) Levels

	Fe	O	Por	SH	C_3H_6
			Bond Activation TS (**TS1**/**TS1′**)		
^{2}**TS1** [a]	1.69 (1.70)	0.22 (0.21)	−0.28 (−0.26)	−0.32 (−0.32)	−0.31 (−0.33)
^{4}**TS1** [a]	1.19 (1.21)	0.88 (0.84)	0.13 (0.12)	0.42 (0.43)	0.38 (0.40)
^{4}**TS1′**	3.72 (3.72)	0.22 (0.24)	0.14 (0.12)	−0.81 (−0.80)	−0.27 (−0.28)
^{6}**TS1′**	3.65 (3.68)	0.20 (0.21)	0.56 (0.55)	0.82 (0.81)	−0.23 (−0.25)
			Radical Intermediate (**2**/**2′**)		
^{2}**2** [a]	1.83 (1.85)	0.31 (0.30)	−0.14 (−0.13)	−0.13 (−0.14)	−0.87 (−0.88)
^{4}**2** [a]	1.85 (1.87)	0.32 (0.29)	−0.13 (−0.14)	0.05 (0.05)	0.91 (0.93)
^{4}**2′**	4.00 (4.00)	0.40 (0.40)	0.31 (0.30)	−0.84 (−0.83)	−0.86 (−0.87)
^{6}**2′**	3.97 (3.99)	0.39 (0.39)	0.69 (0.68)	0.81 (0.81)	−0.86 (−0.87)
			Rebound TS (**TS2**/**TS2′**)		
^{2}**TS2** [a]	− (−)	− (−)	− (−)	− (−)	− (−)
^{4}**TS2** [a]	2.20 (2.22)	−0.01 (−0.01)	−0.12 (−0.14)	0.22 (0.22)	0.71 (0.72)
^{4}**TS2′**	3.89 (3.87)	0.36 (0.34)	0.09 (0.11)	−0.75 (−0.75)	−0.60 (−0.56)
^{6}**TS2′**	3.96 (3.97)	0.32 (0.31)	0.65 (0.62)	0.66 (0.68)	−0.65 (−0.58)
			Product Complex (**3**/**3′**)		
^{2}**3** [a]	1.11 (1.10)	0.00 (−0.01)	−0.09 (−0.08)	−0.02 (−0.02)	0.00 (0.01)
^{4}**3** [a]	2.56 (2.60)	0.02 (−0.03)	−0.02 (−0.03)	0.44 (0.46)	0.00 (0.01)
^{4}**3′**	3.13 (3.14)	0.01 (−0.02)	0.04 (0.06)	−0.18 (−0.19)	0.01 (0.00)
^{6}**3′**	4.00 (4.04)	0.02 (−0.03)	0.51 (0.49)	0.47 (0.49)	0.00 (0.01)

[a] B1 data taken from ref 5c.

O- - -H- - -C; ^{4}**TS3** being the latest (highest degree of C−H cleavage), ^{6}**TS3′** the earliest (lowest degree of C−H cleavage), while the other two species are in between.

4. Discussion

There are a number of interesting features in the reactivity of the penta-radicaloid states of Cpd I. First, why are their energies getting lower compared with those of the tri-radicaloid states along the reaction path? Second, what is the reason for the upright conformations of the bond activation TSs, as opposed to the more sideways-type conformations of the species derived from the reactions of the tri-radicaloid states? Why are the penta-radicaloid states so affected by the environment, such as hydrogen bonding to the thiolate ligand and polarization by a dielectric medium? What is the mechanistic significance of the spin density changes? And finally, what are the mechanistic

Table 3. Group Spin Densities during Hydroxylation at the B3LYP/B1 and B3LYP/B2//B1 (in Parentheses) Levels

	Fe	O	Por	SH	C_3H_6
			Bond Activation TS (**TS3**/**TS3′**)		
^{2}**TS3** [a]	1.73 (1.75)	0.10 (0.09)	−0.29 (−0.28)	−0.19 (−0.19)	−0.35 (−0.36)
^{4}**TS3** [a]	1.20 (1.22)	0.74 (0.72)	0.19 (0.17)	0.40 (0.41)	0.47 (0.48)
^{4}**TS3′**	3.81 (3.80)	0.23 (0.24)	0.17 (0.16)	−0.83 (−0.82)	−0.38 (−0.39)
^{6}**TS3′**	3.77 (3.77)	0.19 (0.21)	0.61 (0.58)	0.81 (0.82)	−0.37 (−0.37)
			Radical Intermediate (**4**/**4′**)		
^{2}**4** [a]	1.80 (1.83)	0.29 (0.27)	−0.11 (−0.14)	0.01 (0.02)	−0.99 (−0.98)
^{4}**4** [a]	1.81 (1.82)	0.30 (0.27)	−0.12 (−0.12)	0.02 (0.02)	0.99 (1.01)
^{4}**4′**	4.04 (4.04)	0.43 (0.42)	0.36 (0.38)	−0.85 (−0.87)	−0.97 (−0.97)
^{6}**4′**	4.00 (4.01)	0.43 (0.42)	0.72 (0.72)	0.82 (0.82)	−0.97 (−0.98)
			Rebound TS (**TS4**/**TS4′**)		
^{2}**TS4** [a]	− (−)	− (−)	− (−)	− (−)	− (−)
^{4}**TS4** [a]	2.15 (2.15)	0.02 (0.03)	−0.12 (−0.15)	0.14 (0.14)	0.81 (0.83)
^{4}**TS4′**	4.00 (4.01)	0.38 (0.36)	0.23 (0.25)	−0.80 (−0.81)	−0.80 (−0.80)
^{6}**TS4′**	3.99 (4.00)	0.38 (0.35)	0.69 (0.67)	0.75 (0.76)	−0.80 (−0.78)
			Product Complex (**5**/**5′**)		
^{2}**5** [a]	1.09 (1.09)	0.00 (0.00)	−0.08 (−0.09)	−0.01 (−0.01)	0.00 (0.00)
^{4}**5** [a]	2.99 (3.01)	0.01 (−0.01)	0.05 (0.06)	−0.05 (−0.06)	0.00 (0.00)
^{4}**5′**	3.14 (3.14)	0.01 (0.00)	0.04 (0.05)	−0.20 (−0.20)	0.00 (0.00)
^{6}**5′**	4.00 (4.04)	0.03 (−0.02)	0.50 (0.49)	0.48 (0.49)	0.00 (0.00)

[a] B1 data taken from ref 5c.

implications of the interference of the penta-radicaloid states in the reactivity of Cpd I?

To answer these questions we need to analyze the electronic reorganization during the reactions (see Tables 1−3 and Scheme 3) and the associated changes in the exchange interactions and orbital energy gaps.[23] The exchange interactions between electrons of the same spin stabilize higher-spin states over lower ones, while increasing orbital energy gaps favor lower-spin states with electrons paired in doubly occupied orbitals. The important exchange interactions are those between electrons on the same moiety, and hence we shall focus only on the interactions between the electrons in the d orbitals of iron, while neglecting such interactions between electrons on spatially separated moieties, e.g., one in a d orbital and the other in an orbital on propene or on porphyrin. The d−d exchange interactions of iron are quite large, e.g., 19−21 kcal/mol in the case of Fe^+.[23] Thus, as the number of d−d exchange interactions accumulates, the exchange stabilization of the high-spin states increases significantly and these states will become competitive with low-spin ones. In the case of Cpd I, the penta-radicaloid states have six d−d exchange interactions vs only one for the tri-radicaloid states (see Scheme 1). This is the reason the penta-radicaloid states are no more than 12 kcal/mol above the tri-radicaloids Cpd I, even though the $\delta \rightarrow \sigma^*_{xy}$ excitation energy is significant. Such small gaps were also found in correlated ab initio calculations on small model systems analogous to Cpd I,[7] and we may therefore conclude that B3LYP is realistic in this regard.

Scheme 3 provides the basis for the qualitative discussion of the exchange effects during epoxidation and hydroxylation. For each of the four states considered (nascent from ^{2}**1**,^{4}**1**,^{4}**1′**,^{6}**1′**) it shows the orbital occupation patterns in reactant, intermediate, and product, as well as their changes during bond activitation and rebound. The orbital occupations were extracted from the natural orbitals (NO) computed at the B3LYP/B1 level (see Figures S3−S7 of Supporting Information for some representative examples). Singly occupied orbitals in Scheme 3 are characterized by NO occupation numbers close to 1 which leads to a maximum of seven such orbitals in the hepta-radicaloid rebound intermediates (Scheme 3, c and d). The orbitals in Scheme 3 are given simple labels to indicate their character, but they are generally delocalized, of course; for example "a_{2u}" extends over the porphyrin and thiolato ligands, "ϕ_C" and "$\sigma^*_{z^2}$" are normally mixed, and σ^*_{xy} contains contributions from the pyrrole nitrogen atoms. Due to such delocalization, the actual spin densities at iron (Tables 1−3) tend to be smaller than anticipated from the simple representations in Scheme 3, but they follow the same trends. We can thus use the simplified orbital occupation pattern in Scheme 3 for rationalizing the changes in d−d exchange effects during the reactions.

According to Scheme 3, which is based on the oxidation-state formalism,[3] Cpd I stores two oxidation equivalents above the resting state or the product complex; one oxidation equivalent is on the iron center which is a high-valent, Fe^{IV} species, the other resides in the porphyrin (Por), which appears as a radical cationic state, $Por^{\bullet+}$. During the oxidation process, the $Fe^{IV}Por^{\bullet+}$ moiety "gains" two electrons from the substrate and is transformed to $Fe^{III}Por$. This electron flow for the tri-radicaloid states was described before,[3,5a−d] and is repeated in Scheme 3, a and b, using the orbitals of the oxo−iron porphyrin and one orbital of the propene substrate; σ_{CH} type for hydroxylation and $\pi_{C=C}$ type for epoxidation. Thus, the bond activation process is attended by an electron shift from the corresponding propene orbital to the singly occupied a_{2u} orbital to fill the porphyrin radical cationic hole. In the rebound step the remaining electron on the radical center (in ϕ_C) is shifted into one of the d orbitals on iron, to π^*_{xz} in the case of the doublet process, and into $\sigma^*_{z^2}$ in the case of the quartet process. Note that the quartet products nascent from ^{4}**1′** and ^{4}**1** differ in their orbital occupations (Scheme 3, b and c) and are therefore different species.

In the case of the penta-radicaloid states (Scheme 3, c and d), the electron is shifted into $\sigma^*_{z^2}$ during bond activation and thereby creates *hepta-radicaloid intermediates*, ^{4}**2′**, ^{6}**2′**, ^{4}**4′**, and ^{6}**4′**. As may be seen from Tables 2 and 3, this causes a rise of the spin density at iron and the porphyrin, in the bond activation TSs, ^{4}**TS1′**, ^{6}**TS1′**, ^{4}**TS3′**, and ^{6}**TS3′**, as well as in the respective

(23) Carter, E. A.; Goddard, W. A., III. *J. Phys. Chem.* **1988**, *92*, 5679−5683.

Scheme 3. Electronic Reorganization during Epoxidation and Hydroxylation by the Tri-radicaloid and Penta-radicaloid States[a]

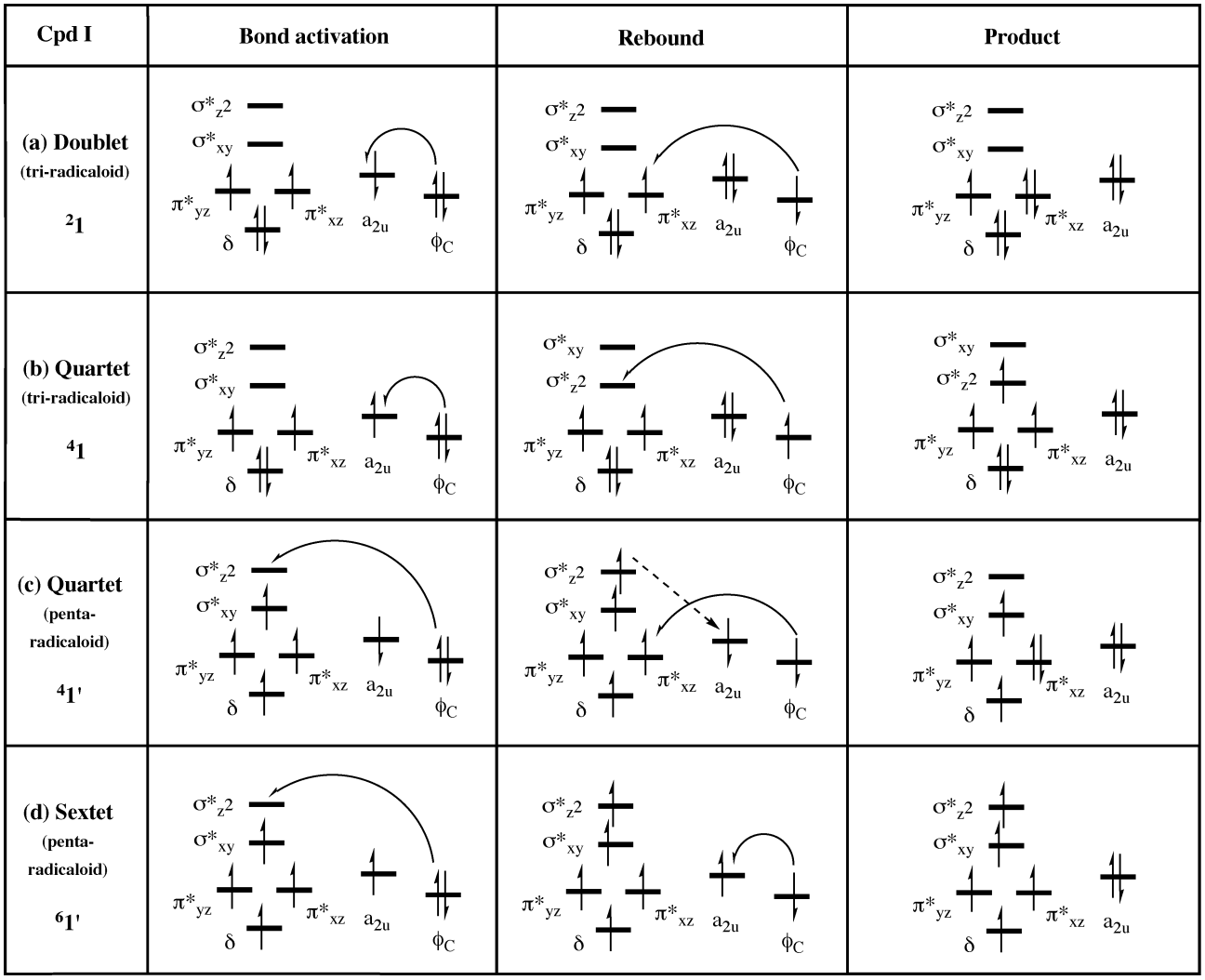

[a] The dotted arrow in (c) signifies that the electron that is shifted initially to $\sigma^*_{z^2}$ is demoted to a_{2u} in the rebound step, enhanced by the mixed character of these orbitals.

intermediates, ^{4}**2′**, ^{6}**2′**, ^{4}**4′**, and ^{6}**4′**. Generation of the hepta-radicaloid species leads to significant increase in the number of d−d exchange interactions on the iron, formally from six in ^{6,4}**1′** to 10 in ^{4}**2′**, ^{6}**2′**, ^{4}**4′**, and ^{6}**4′**. Since the d−d exchange interactions on iron are quite large,[23] the additional exchange interactions stabilize the hepta-radicaloid species relative to the original penta-radicaloid species in ^{6}**1′** and ^{4}**1′** and even more so compared with the species generated from the tri-radicaloid states. Therefore, it is the exchange stabilization that causes shrinkage of the energy gaps between the multi-radicaloid states (penta- and hepta-) and the tri-radicaloids, from 12 to 13 kcal/mol in the reactants to 6 kcal/mol or less for the intermediate stage.

Environmental effects increase this differential stabilization, thereby causing the sextet intermediate to move close to or even below the doublet species in energy (Figure 8). The reason for this additional stabilization of the high-spin states was analyzed before[17a,b] and attributed to the stabilization of the $\sigma^*_{z^2}$ orbital by electrostatic interactions and hydrogen bonding to sulfur. The orbital model presented in Scheme 4 shows that the $\sigma^*_{z^2}$ orbital is lower in a polar environment compared with the gas phase due to the weaker mixing between the thiolate ligand and the d_{z^2} orbital on the iron. Since the $\sigma^*_{z^2}$ orbital gets filled in the stage of the hepta-radicaloid intermediates, these intermediates are stabilized more, compared with the doublet-state species, in which the $\sigma^*_{z^2}$ orbital is vacant. Furthermore, the long Fe−S bonds of the hepta-radicaloid intermediates and the higher negative charge on the thiolate ligand further accentuate the polarity-induced stabilization of these complexes relative to the tri-radicaloid intermediates. The same considerations apply to the different spin states of the product complexes, depending on the occupancy in the $\sigma^*_{z^2}$ orbital.

Another mark of the electron shift into the $\sigma^*_{z^2}$ orbital, during bond activation in the penta-radicaloid pathways, is the upright conformation of ^{6}**TS1′**/^{4}**TS1′** and ^{6}**TS3′**/^{4}**TS3′**, compared with their tri-radicaloid analogues (see Figures 3 and 4). The upright conformation arises due to the tendency to attain maximum overlap between the propene orbital and the accepting orbital in the iron−oxo porphyrin moiety.[3a] However, in the case of the penta-radicaloid quartet spin state, past the intermediates the electron that is initially shifted to the $\sigma^*_{z^2}$ orbital is demoted to a_{2u} in the rebound step (as shown by the dotted arrow in Scheme 3c) since the two orbitals maintain overlap (due to the fact that the sulfur hybrid orbital contributes to both).[18]

Scheme 4. Orbital Interaction Diagrams Showing the Formation of the $\sigma^*_{z^2}$ Orbital in the Gas Phase (to the right) and in a Polar Environment (to the left) by Mixing of the Hybrid Orbital on the Sulfur, the σ_S Orbital, and the d_{z^2} Orbital on Iron[a]

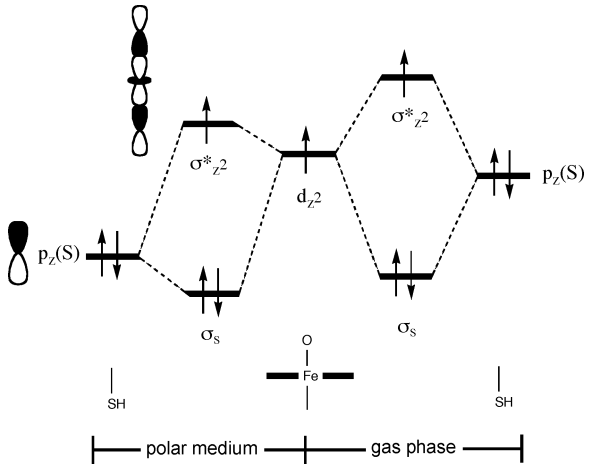

[a] Note that the sulfur hybrid is stabilized by the polar environment and by direct NH- - -S hydrogen bonds, and as a result it interacts less strongly with the d_{z^2} orbital, thus producing a lower $\sigma^*_{z^2}$ orbital compared with the gas-phase situation.

Another aspect in Figures 6−8 is concerned with the barriers for rebound and ring closure. These trends were explained before for the tri-radicaloid states.[3a] Thus, the following principles were established: (a) In the doublet state, Scheme 3a, an electron is shifted from the radical center, ϕ_C, to a low-lying π^*_{xz} orbital, and the two orbitals that participate in the electron shift can maintain a significant overlap that facilitates the rebound and/or ring closure, leading to a barrier-free process. (b) The small barrier in the quartet tri-radicaloid rebound processes, Figures 6−8, arises since in Scheme 3b the electron shifts from ϕ_C to the higher-lying $\sigma^*_{z^2}$ orbital, while the Fe−O bond is still short with significant Fe−O antibonding interaction (the barrier is mitigated by generation of two exchange interactions, and hence it is not too large). Interestingly, the two penta-radicaloid states possess significant rebound and ring closure barriers, even though the electron is shifted from ϕ_C to low-lying orbitals.

Thus, in Scheme 3c, the electron shifts to the π^*_{xz} orbital as in Scheme 3a, but nevertheless, the penta-radicaloid state exhibits a barrier, as opposed to the barrier-free processes in the tri-radicaloid states. On the basis of the principles discussed so far, the reason for the rebound barrier for the process in Scheme 3c is that the electron shift to the π^*_{xz} orbital and the concurrent demotion of the electron from $\sigma^*_{z^2}$ to a_{2u} reduce the number of exchange interactions from 10 in the intermediate to 3 in the rebound ^{4}**TS′** species. This appreciable loss of exchange stabilization induces a barrier.

In a similar vein, the rebound process for the sextet penta-radicaloid state has a barrier even though the electron is shifted to the a_{2u} orbital, which is low-lying; such a shift in the low-spin doublet rebound has a tiny barrier if at all.[24] Let us focus on the rebound in the epoxidation process and compare ^{2}**2**-Fe(III) to ^{6}**2′**.[5b] An obvious difference between the Fe^{III} doublet-state intermediate and the sextet one is that in the latter the d-shell is half-filled, and therefore during rebound, the electron that is shifted to a_{2u} encounters repulsion with the half-filled shell of the iron and produces a barrier. Another difference is the Fe−S bond length, which is much longer in the penta-radicaloid intermediate ^{6}**2′** than in the doublet state, ^{2}**2**-Fe(III). The orbitals of the two species will be affected by this geometric difference; thus, as a result of the Fe−S bond lengthening, the singly occupied "a_{2u}" orbital of ^{6}**2′** concentrates more on the thiolate ligand with little amplitude on the porphyrin (see Supporting Information). Consequently, the orbital gets disjoined from the radical orbital ϕ_C, such that their overlap diminishes. By contrast, in the ^{2}**2**-Fe(III) intermediate the "a_{2u}" and ϕ_C orbitals are mixed (see Supporting Information), and their overlap is significant. The diminished orbital overlap in ^{6}**2′** contributes to a rebound barrier for this state.

Mechanistic Implications. The multistate picture of reactivity in Figures 5−8 still obeys the same basic rules as observed before.[3,5,24,25] In both hydroxylation and epoxidation, the low-spin doublet-state process proceeds in an effectively concerted manner toward products, while all the other states, with higher spin quantum number, have truly stepwise mechanisms with finite barriers for rebound or ring closure. In addition to the tri-radicaloid intermediates, ^{2}**2**, ^{4}**4**, which are shown here in Figures 6−8, and which correspond to iron in oxidation state IV, Fe(IV), there exist the Fe(III) electromers,[3,24,25] which are not shown in the figures but follow the same basic rules. Thus, *the region of the intermediates has a dense manifold of six different states*. In the case of chiral or stereochemically labeled substrates (i.e., chiral C−H centers, or cis and trans double bonds), this interplay of the intermediate states will result in some stereochemical scrambling, depending on the interconversion dynamics of the different intermediate states. This dynamics will depend on relative energies of the intermediates, the barriers for rearrangements, as well as on the rates of spin-flips among the spin states.[26]

A potentially useful probe for the spin states is the KIE ratio for the different products (i.e. the product isotope effect, PIE)[5e,25] produced during the hydroxylation processes of stereochemically labeled substrates. Thus, since the low-spin process is the only one that proceeds via an effectively concerted hydroxylation, while the higher spin-states proceed by stepwise mechanisms where the labeled allylic radical can rearrange during its finite lifetime, the products with conserved stereochemistry will reflect the KIE for the low-spin (LS) process, KIE_{LS}, while the products with scrambled stereochemistry will reflect the KIE of the higher-spin states, KIE_{HS}. In a scenario where the only reactive species are nascent from the tri-radicaloid states, the PIE ratio [KIE_{LS}/KIE_{HS}] will be 0.848/0.732 using the Eyring/Wigner-corrected KIE values (see section 3.4). However, in a scenario as predicted by the results of Figure 8, where the sextet state is the lowest intermediate, the PIE ratio, [KIE_{LS}/KIE_{HS}], will be determined by the doublet and the sextet states and is 1.057/1.092. Of course, while the product isotope effect is substrate dependent,[5e] the strategy itself is general and may be useful as an experimental probe of the spin-state situation.

5. Conclusion

Our DFT results suggest that the reactivity of Cpd I of P450 might well be influenced by the penta-radicaloid states of the sextet and quartet spin variety, which arise from the ground state by a $\delta \rightarrow \sigma^*_{xy}$ orbital excitation within the d manifold.

(24) Schöneboom, J. C.; Cohen, S.; Lin, H.; Shaik, S.; Thiel, W. *J. Am. Chem. Soc.* **2004**, *126*, 4017−4034.
(25) Shaik, S.; de Visser, S. P.; Kumar, D. *J. Biol. Inorg. Chem.* **2004**, *9*, 661−668.
(26) Danovich, D.; Shaik, S. *J. Am. Chem. Soc.* **1997**, *119*, 1773−1786.

B3LYP calculations show that the energies of these states become very low along the reaction pathways for hydroxylation and epoxidation, due to the increase of the exchange interactions in the open-shell d block. Furthermore, these states are stabilized relative to tri-radicaloid ground states by the polar environment and hydrogen bonding to the thiolate ligand. As such, in the active site of P450s, these states may become accessible and contribute to the multistate reactivity[27] of Cpd I. Electric fields can be utilized to further control the relative energy of these intermediates and hence manipulate their relative poulation and rates of interconversion.[28] Studies of product isotope effects[5e,25] may help probing the participation of the penta-radicaloid states. Deciphering the reaction dynamics among all the spin- and electromeric states of the reaction intermediates is a challenge for experiment and theory.

Finally, a sober note of caution is necessary to emphasize again the limited accuracy of the DFT-B3LYP approach for relative energies of spin states. Clearly, higher-level ab initio calculations[7,16] will be required eventually for assessing the importance of the higher-spin states in the chemistry of P450 enzymes. Despite this caveat, the qualitative conclusions on the role of d−d exchange effects along the reaction path are expected to remain valid because they reflect the essential electronic reorganization during the reaction.

Acknowledgment. The research at HU was supported by the German Federal Ministry of Education and Research (BMBF) within the framework of the German-Israeli Project Cooperation (DIP), and in part by a grant from the Israel Science Foundation (ISF).

Supporting Information Available: Five tables and seven figures showing group charges and atomic coordinates of the critical species for the reactions of penta-radicaloid Cpd I, relative energies of the resting state, energy profiles, and natural orbitals of intermediate species. This material is available free of charge via the Internet at http://pubs.acs.org.

JA053847+

(27) Kumar, D.; de Visser, S. P.; Shaik, S. *Chem. Eur. J.* **2005**, *11*, 2825−2835.
(28) Shaik, S.; de Visser, S. P.; Kumar, D. *J. Am. Chem. Soc.* **2004**, *126*, 11746−11749.